Tailored the Polymer Interface of Prussian Blue Analogues for Sodium-ion Batteries

Parham Pirayesh[1], Enzhong Jin[1], Yijia Wang[1], Zhi liang Dong[1], Yi Gan[1], Yi Yuan[1], Mingrui Yang[1], Reza Andaveh[1], Frederick Benjamin Holness[1], Shin-An Chen[3], Lo-Yueh Chang[3], Xin Pang[2], Yang Zhao[1]*

[1]Department of Mechanical and Materials Engineering

University of Western Ontario, London, Ontario, N6A 5B9, Canada

Email: Y. Zhao: yzhao628@uwo.ca

[2]CanmetMATERIALS

Natural Resources Canada, 183 Longwood Road South, Hamilton, ON L8P 0A5, Canada.

[3] National Synchrotron Radiation Research Center, Hsinchu 300092, Taiwan

Experimental Section

Synthesis of Prussian Blue (PB)

All chemicals for synthesizing PBAs in laboratory were purchased from Australian Sigma Aldrich, and PB samples were synthesized via a modified coprecipitation method at 25 °C under a nitrogen (N_2) atmosphere to prevent Fe^{2+} oxidation. Two precursor solutions were prepared: Solution A contained 7.5 g of sodium citrate and 1.67 g of $FeSO_4 \cdot 7H_2O$ dissolved in 100 mL of deionized water, while Solution B contained 7.5 g of sodium citrate and 1.96 g of $Na_4Fe(CN)_6 \cdot 10H_2O$ in 100 mL of deionized water. Both solutions were purged with N_2 gas for 3 h under stirring. Solution A was then added dropwise into Solution B at a controlled rate of 0.83 mL min^{-1}. The mixture was stirred for an additional 6 h and subsequently aged overnight. The resulting precipitate was collected by centrifugation, washed three times with deionized water and once with ethanol, and dried in a vacuum oven at 110 °C for 24 h.

Synthesis of Functionalized Linked Polymer (FLP) Coatings via MLD

An FLP coating was deposited on PB powders using a GEMstar-XT ALD system (Arradiance, USA) directly connected to an argon-filled glovebox. Ethylenediamine (ED) and 1,4-phenylene diisocyanate (PDIC) (Sigma-Aldrich) were employed as organic precursors, stored in stainless steel reservoirs. During deposition, the ED reservoir was kept at room temperature, while the PDIC reservoir was heated to 90 °C to ensure sufficient vapor pressure. The MLD chamber was maintained at 65 °C with a processing pressure of ~180 mTorr, using argon as both carrier and purge gas. Each MLD cycle consisted of a 0.1 s ED pulse, a 30 s purge, a 1 s PDIC pulse, and a final 30 s purge. PB powders were coated with 10, 25, and 50 cycles, producing samples denoted PB@10FLP, PB@25FLP, and PB@50FLP, respectively.

Cathode Fabrication

The cathode slurry was prepared by mixing active material (pristine PB or FLP-coated PB), C65 conductive carbon black, vapor-grown carbon fibers (VGCFs), and polyvinylidene fluoride (PVDF) binder in a 7:1:1:1 weight ratio. N-methyl-2-pyrrolidone (NMP) was used as the solvent. The homogeneous slurry was cast onto carbon-coated aluminum foil, dried at 110 °C under vacuum for 12 h, and roll-pressed. Discs (10 mm diameter) were punched out for use as cathodes.

Electrochemical Measurements

Electrochemical performance was evaluated using CR2032 coin-type cells assembled in an argon-filled glovebox (H_2O/O_2 < 0.01 ppm). Each cell consisted of a pristine Na metal disc anode, a PB-based cathode disc, and a Grade GF/B fine membrane filter (Cytiva Whatman) separator. The electrolyte was 1 M $NaClO_4$ dissolved in a 1:1 (v/v) mixture of ethylene carbonate (EC) and diethyl carbonate (DEC) with 5% fluoroethylene carbonate (FEC) additive. Approximately 180 µL of electrolyte was used per cell. Galvanostatic cycling was performed on a Neware battery testing system over 2.0–4.0 V vs. Na/Na^+. Cells were first activated for three cycles at 1C (1C = 170 mA g^{-1}), followed by long-term cycling at 1C and 5C. Rate performance was evaluated at 0.1C, 0.5C, 1C, 2C, 5C, and 10C, before returning to 0.5C. Cyclic voltammetry (CV) was conducted on a Biologic VMP-3 workstation within 2.0–4.0 V at scan rates of 0.1–0.5 mV s^{-1}. Galvanostatic Intermittent Titration Technique (GITT) measurements were carried out on a Land battery system after three activation cycles at 1C, using a 10 min current pulse followed by a 60 min rest. The Na^+ diffusion coefficient (DNa^+) was calculated using the simplified equation:

$$D_{Na^+} = \frac{4}{\pi\tau}\left(\frac{m_B V_M}{M_B S}\right)^2 \left(\frac{\Delta E_s}{\Delta E_t}\right)^2$$

where:

− τ: duration of the current pulse (s)

- mB: active mass of the material (g)

- MB: molar mass of the material (g mol^{-1})

- VM: molar volume of the material (cm^3 mol^{-1})

- S: electrode–electrolyte contact area (cm^2)

- ΔEs: steady-state voltage change in a GITT step (V)

- ΔEt: total voltage change during the current pulse (V)

Material Characterization

Cycled cells were disassembled inside the argon glovebox for *ex situ* characterization. Electrodes were gently rinsed with anhydrous diethylene glycol dimethyl ether to remove residual electrolyte salts, then sealed in argon-filled containers for transfer. X-ray diffraction (XRD) patterns were obtained using a D8 ADVANCE diffractometer with Cu Kα radiation over 10–80° (2θ). Scanning electron microscopy (SEM) images were acquired using a Hitachi 3400N Environmental SEM and Hitachi 4800 SEM at 5 kV. Transmission electron microscopy (TEM) imaging and energy-dispersive X-ray spectroscopy (EDS) mapping were performed on a Cs-corrected Titan Themis G2 300 TEM at 300 kV. Synchrotron-based analyses were conducted at the Taiwan Light Source (TLS): Fe K-edge X-ray absorption near-edge structure (XANES) spectra at the TLS beamline 07A. X-ray photoelectron spectroscopy (XPS) measurements were performed using a Thermo Scientific K-Alpha spectrometer equipped with a monochromatic Al Kα radiation source (1486.6 eV).

Table S1. Comparison of representative state-of-the-art interphase/coating strategies for PBA cathodes in SIBs

Reference	Cathode Material	Coating Type	Thickness (nm)	Cycling Rate	Cycle Number	Capacity Retention (%)	Coulombic Efficiency (%)
[1]	Fe-HCF	Polypyrrole (PPy)	–	200 mA g^{-1}	500	79	94.9
[2]	PB	Polyaniline (PANI)	~20	100 mA g^{-1}	500	93.4	~95
[3]	PB	NaF-rich CEI	~3.8	1C	3000	68.9	~90
[4]	FeCu-PB	CuO coating	5–15	2 A g^{-1}	1500	~70	~99
[5]	MnHCF	CoxB metallic boride	~5	10C	2500	~74	~96
[6]	Prussian White	ZnO coating	~20	1C	200	94.1	~99
[7]	Fe-PB	PTCA organic coating	15–25	1 A g^{-1}	1000	73.4	~99
This work	**Fe-PB**	**FLP polymer coating (MLD)**	**~8**	**5C**	**3000**	**~68**	**~99.8**

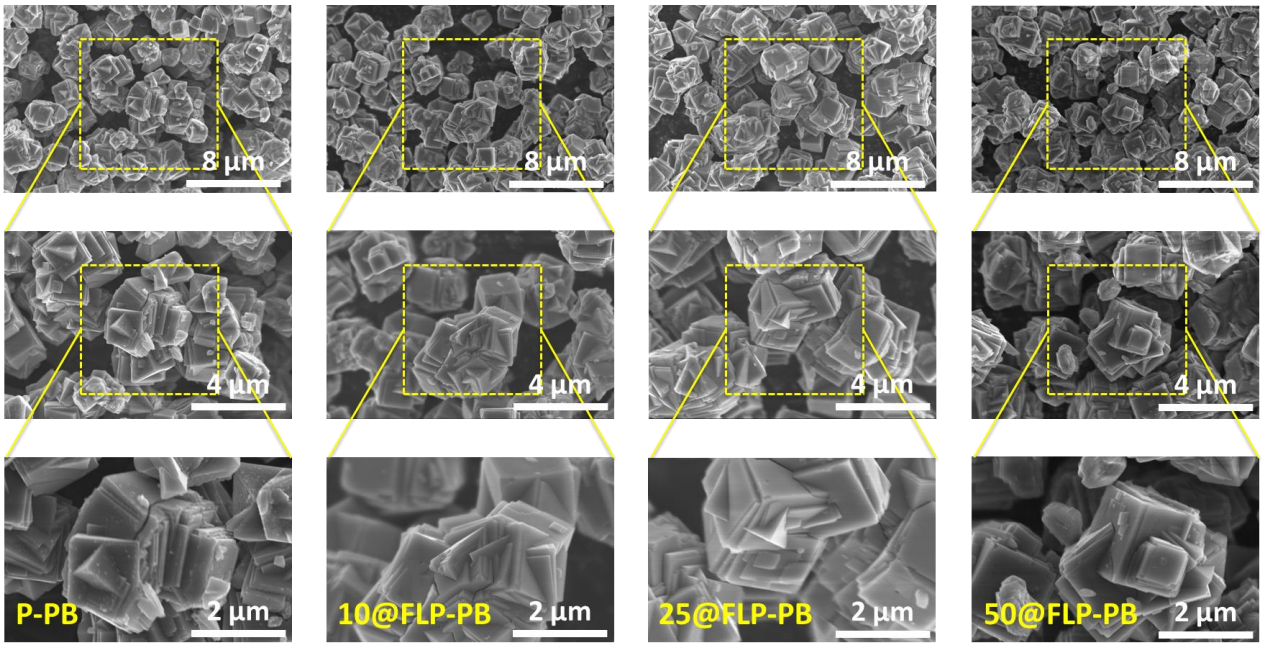

Figure S1. SEM images of P-PB and the FLP-coated cathodes with 10, 25, and 50 MLD cycles, showing the preservation of particle morphology after the coating process.

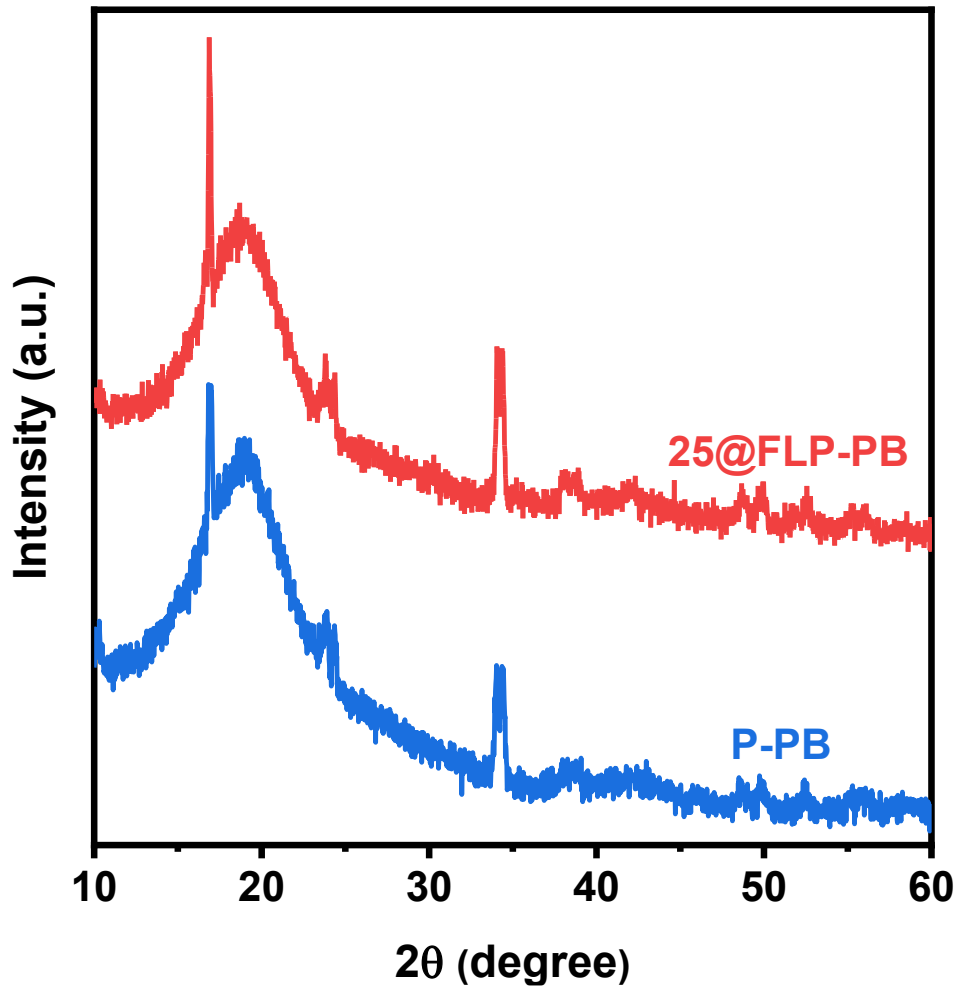

Figure S2. XRD patterns of the P-PB and 25@FLP-PB cathodes, confirming that the MLD process does not alter the bulk crystal structure.

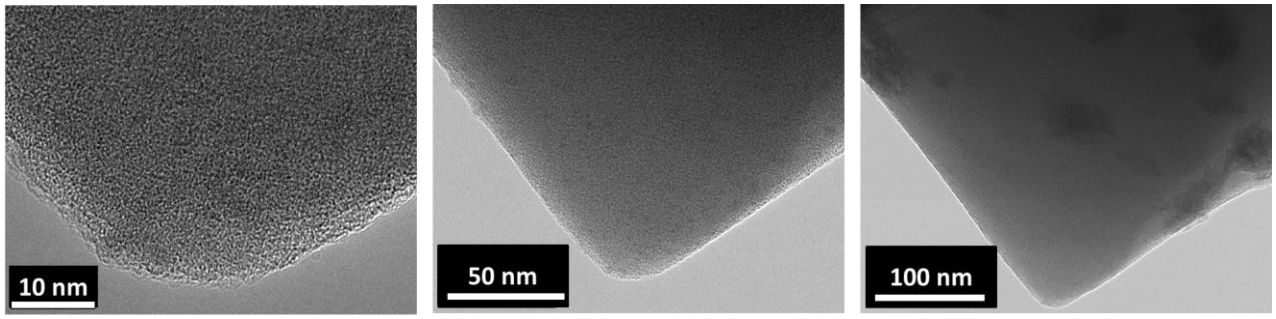

Figure S3. High-resolution TEM image of a P-PB particle, showing a clean, uncoated surface.

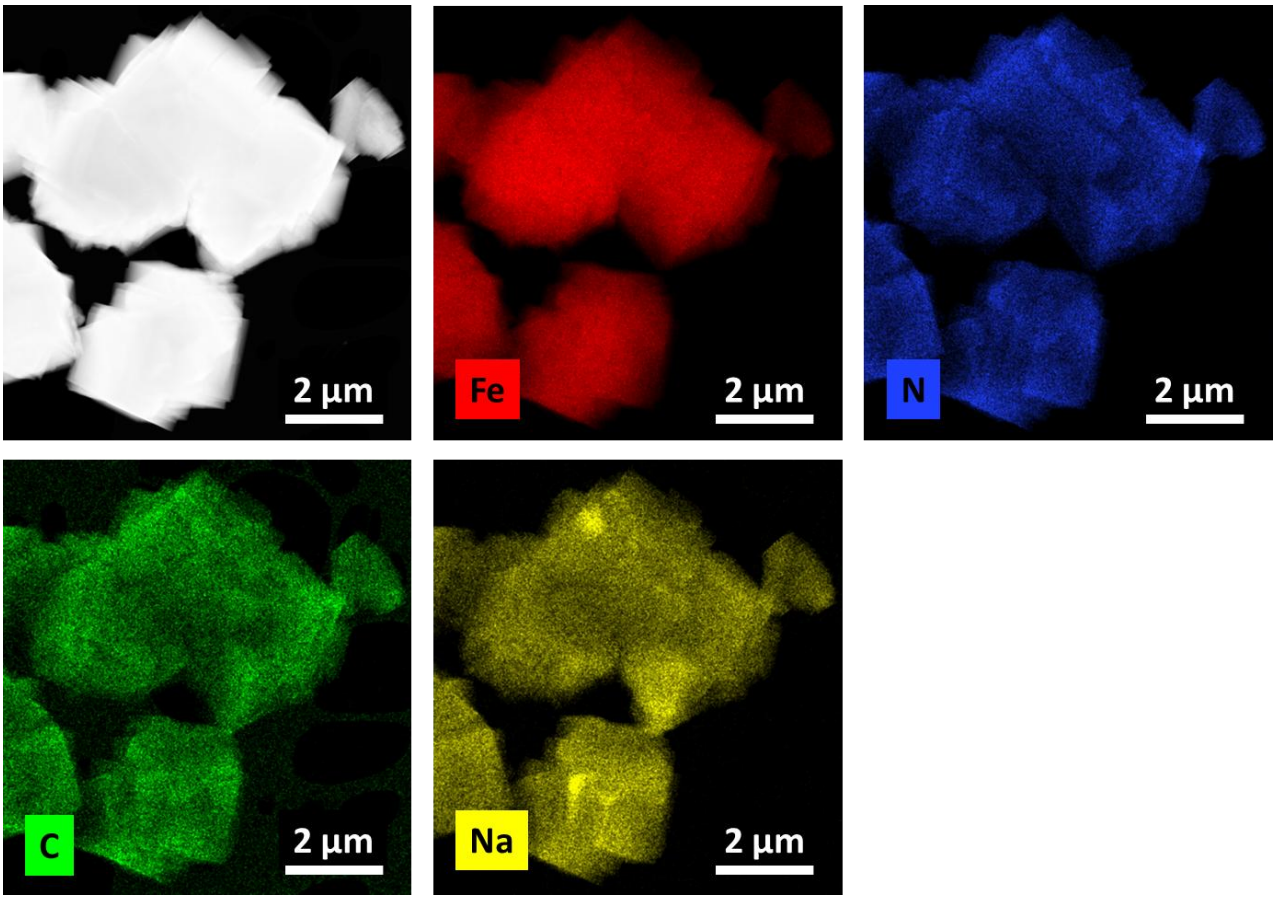

Figure S4. EDS elemental mapping of the P-PB cathode, showing the uniform distribution of framework elements (Fe, N, C).

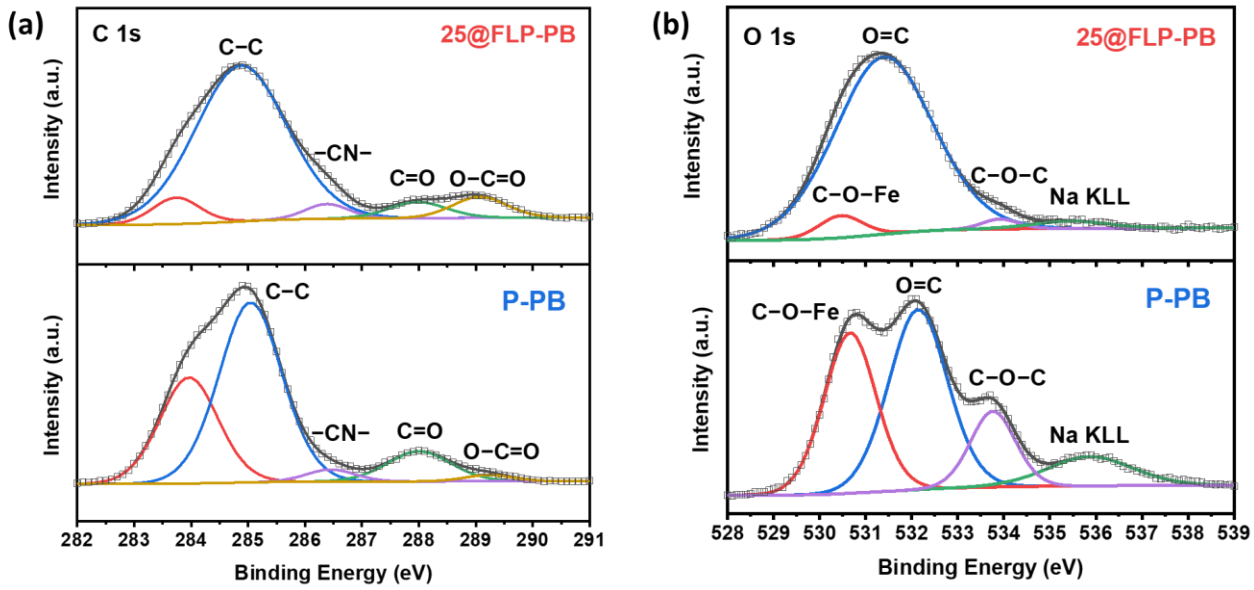

Figure S5. High-resolution XPS spectra for the (a) C 1s and (b) O 1s regions of P-PB and 25@FLP-PB cathodes before cycling.

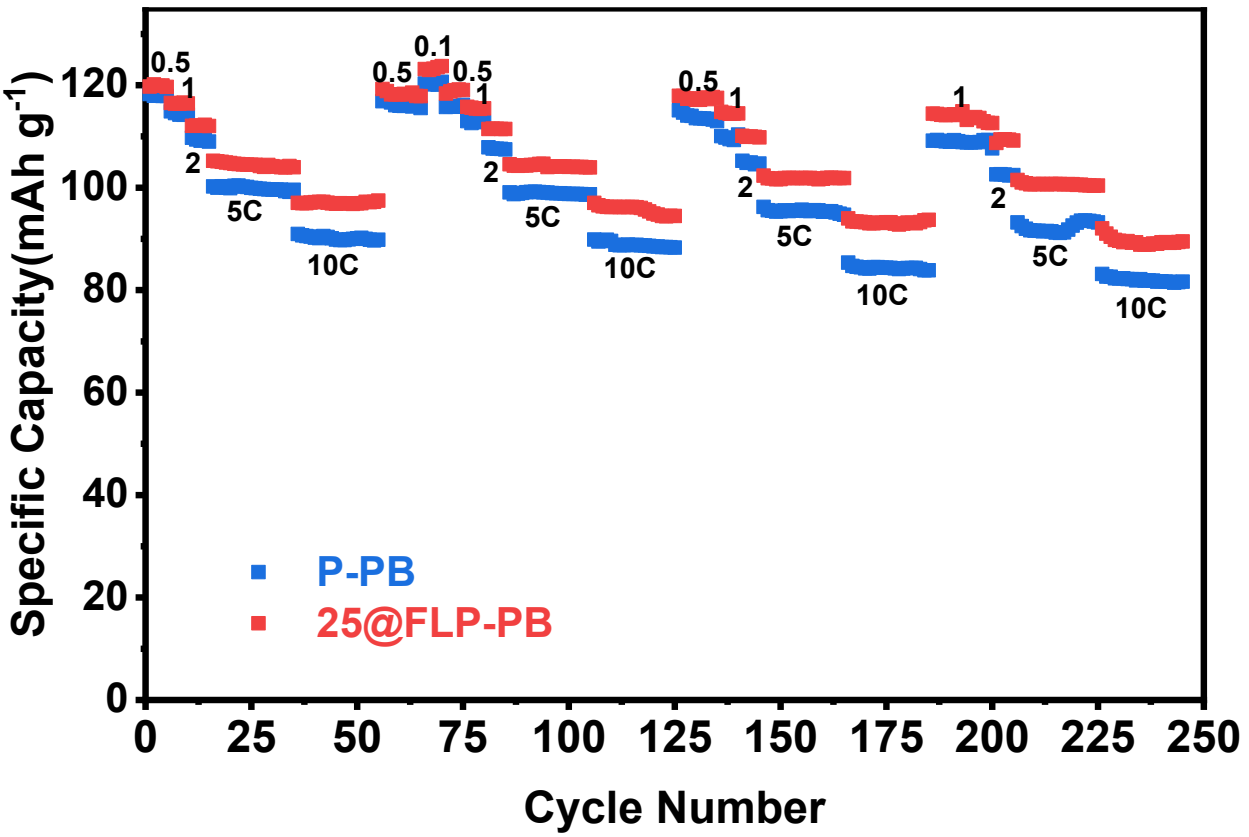

Figure S6. Rate performance of pristine PB and 25@FLP-PB measured stepwise from 0.1C to 10C (repeated sequence).

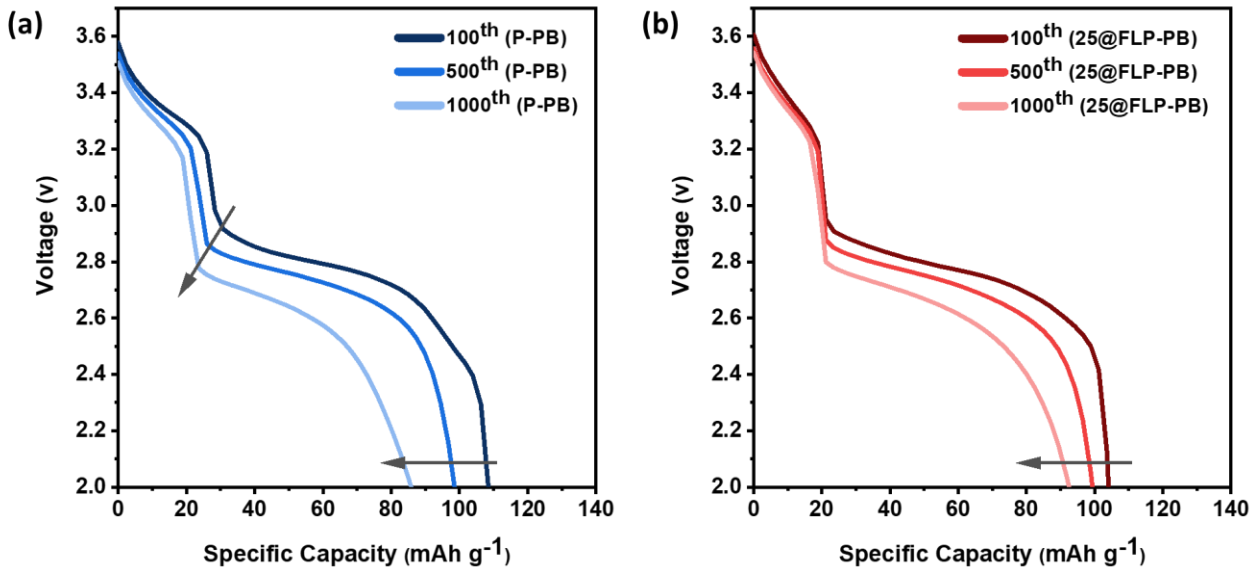

Figure S7. Galvanostatic discharge profiles of (a) P-PB and (b) 25@FLP-PB cathodes at a 5C rate, showing the deconvolution of the total capacity into contributions from the first (low-spin Fe) and second (high-spin Fe) plateaus at the 100^{th}, 500^{th}, and 1000^{th} cycles.

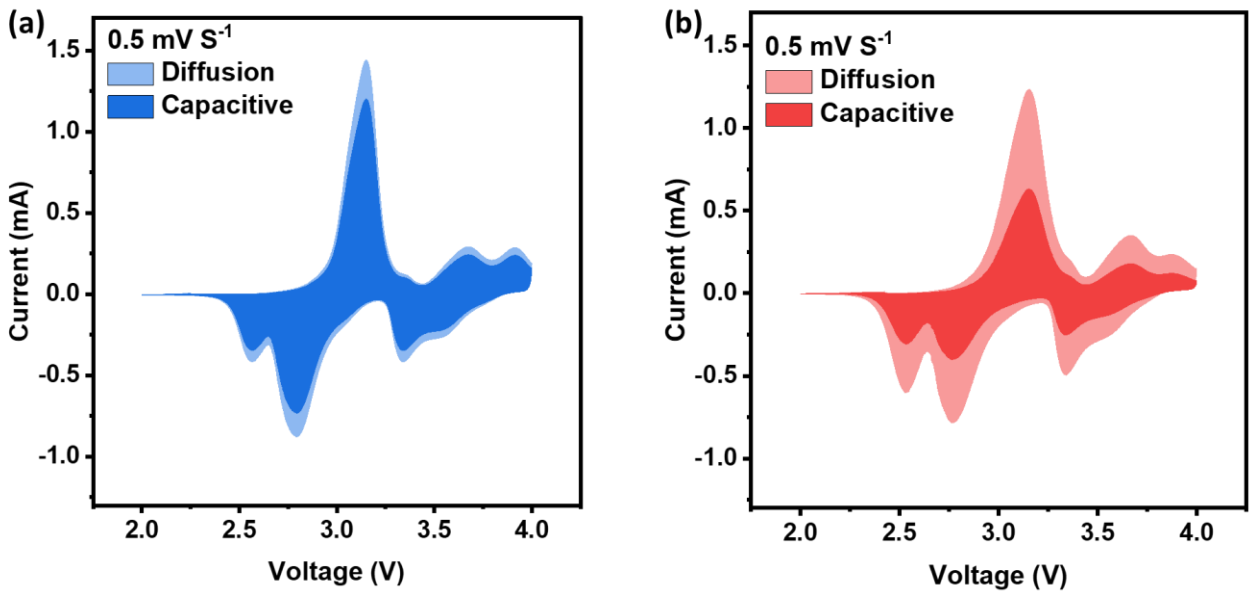

Figure S8. Separation of the capacitive and diffusion currents in (a) P-PB and (b) 25@FLP-PB electrodes at a scan rate of 0.5 mV s^{-1}.

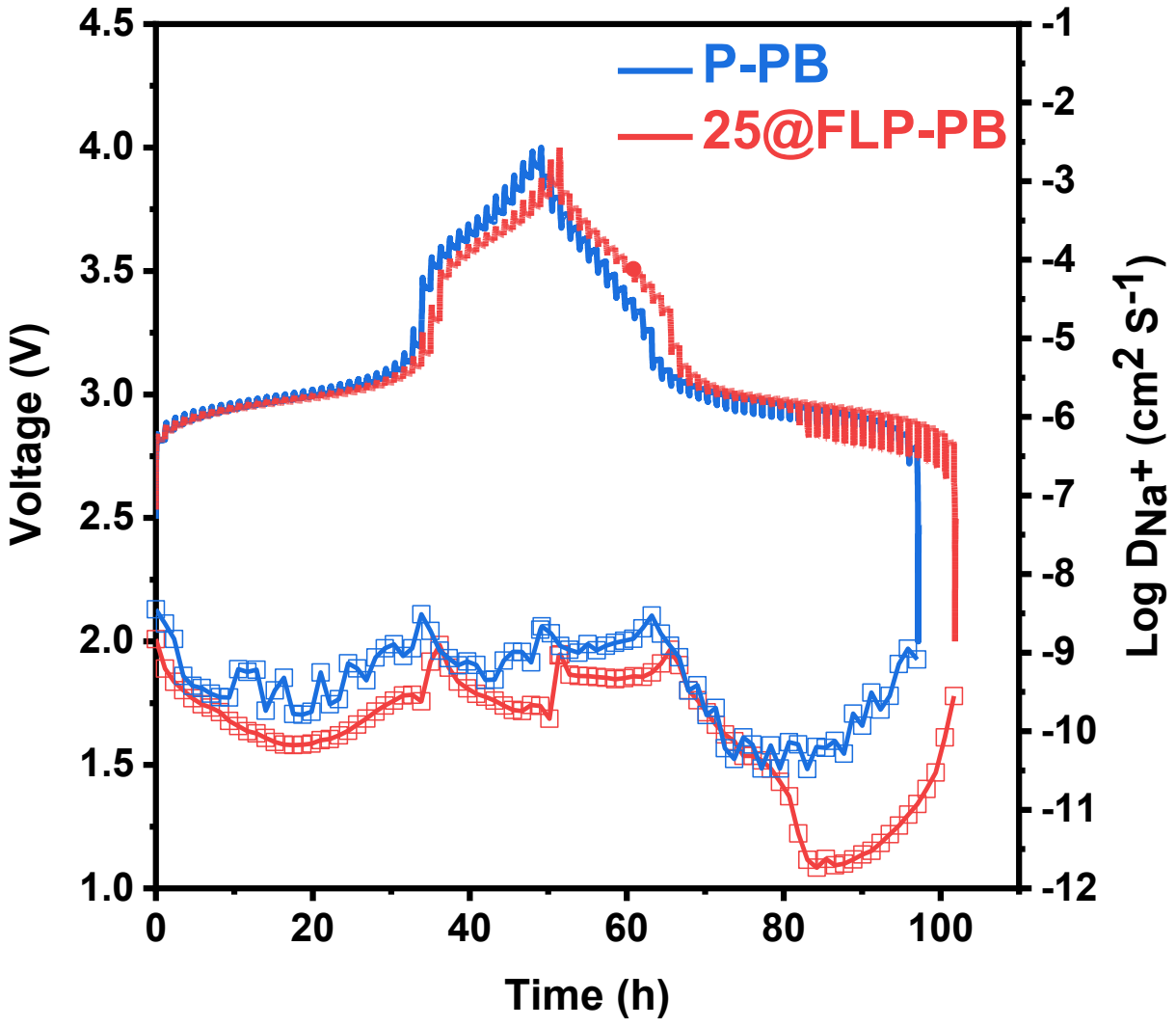

Figure S9. GITT curves and calculated D_{Na}^{+} during the discharge process of P-PB and 25@FLP-PB.

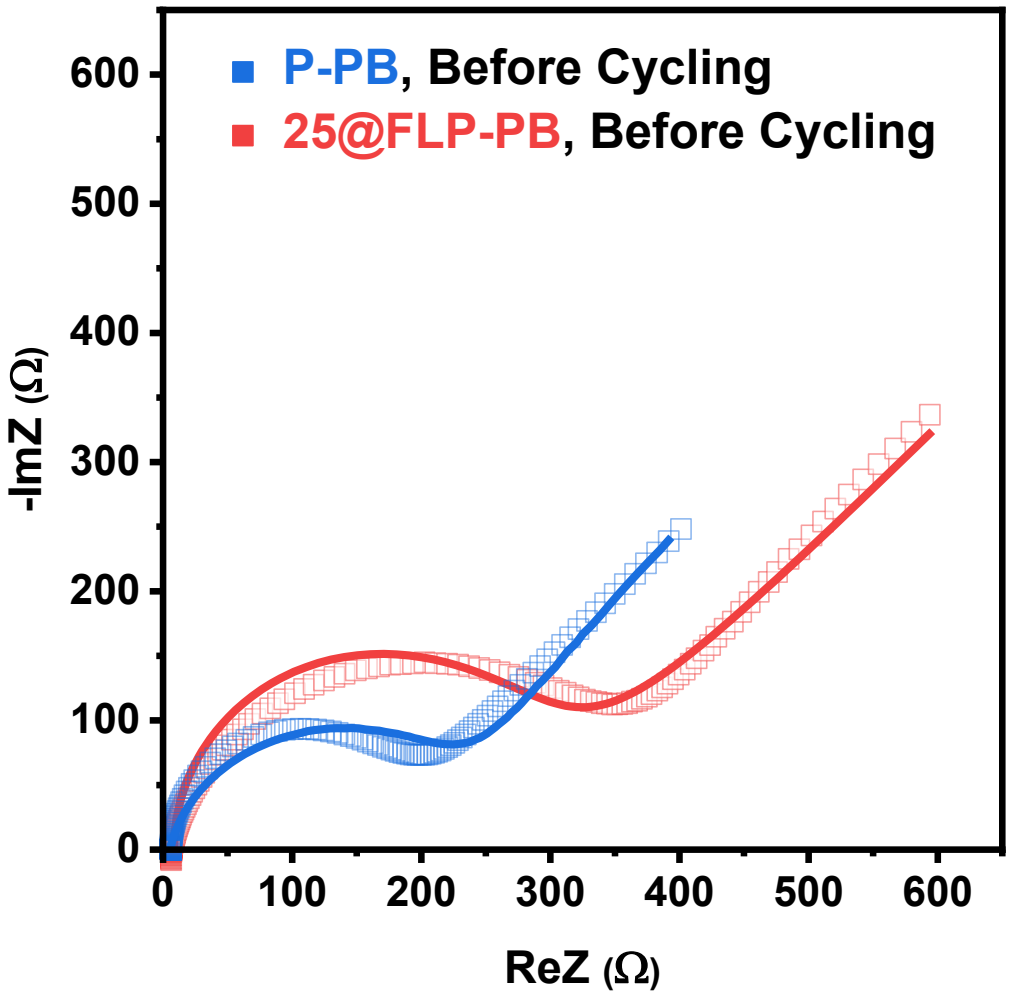

Figure S10. Nyquist plots of P-PB and 25@FLP-PB electrodes before cycling

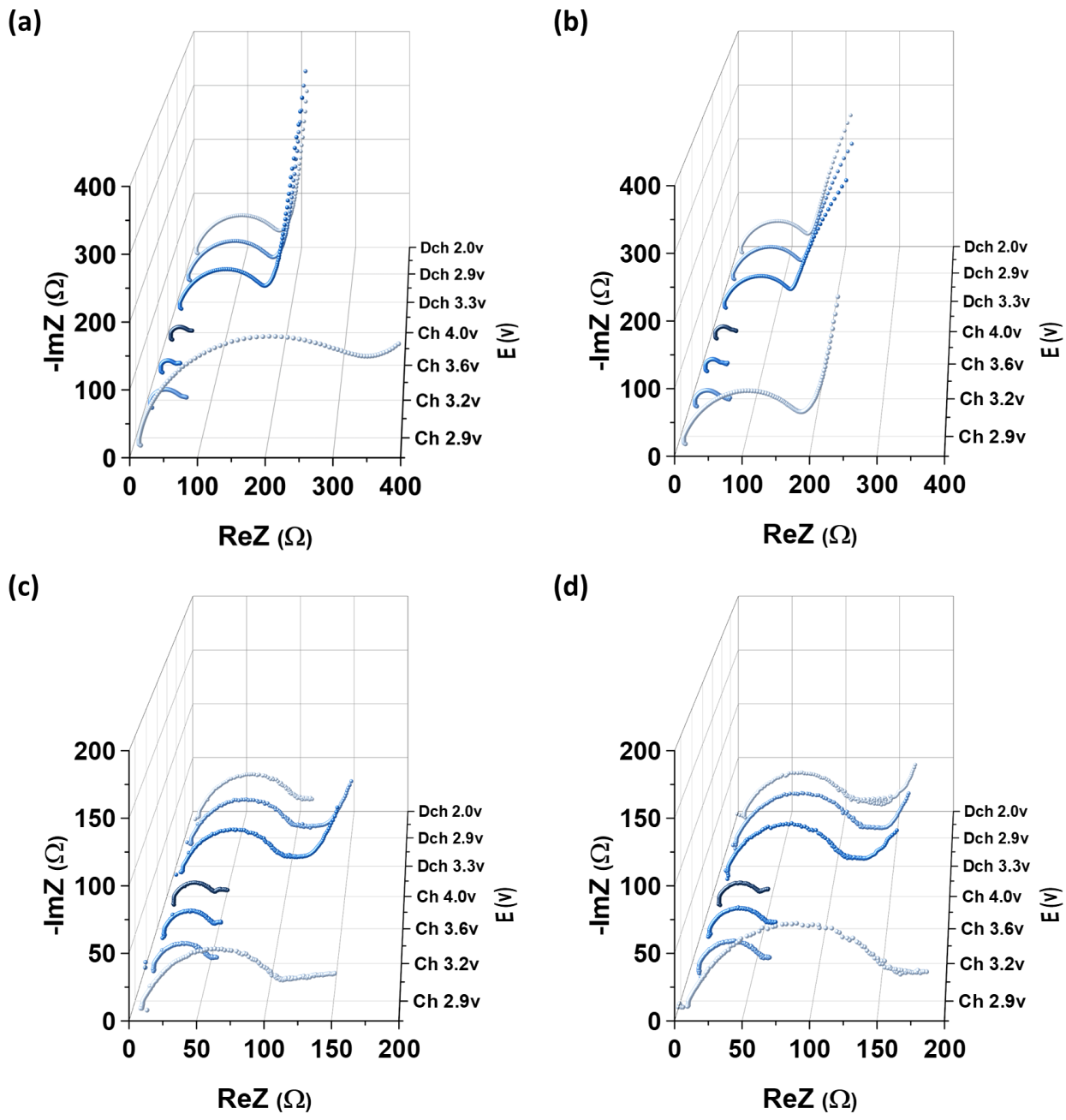

Figure S11. In situ EIS (Nyquist) profiles of pristine PB recorded at selected SOC during the (a) 1st, (b) 2nd, (c) 5th, and (d) 15th cycles.

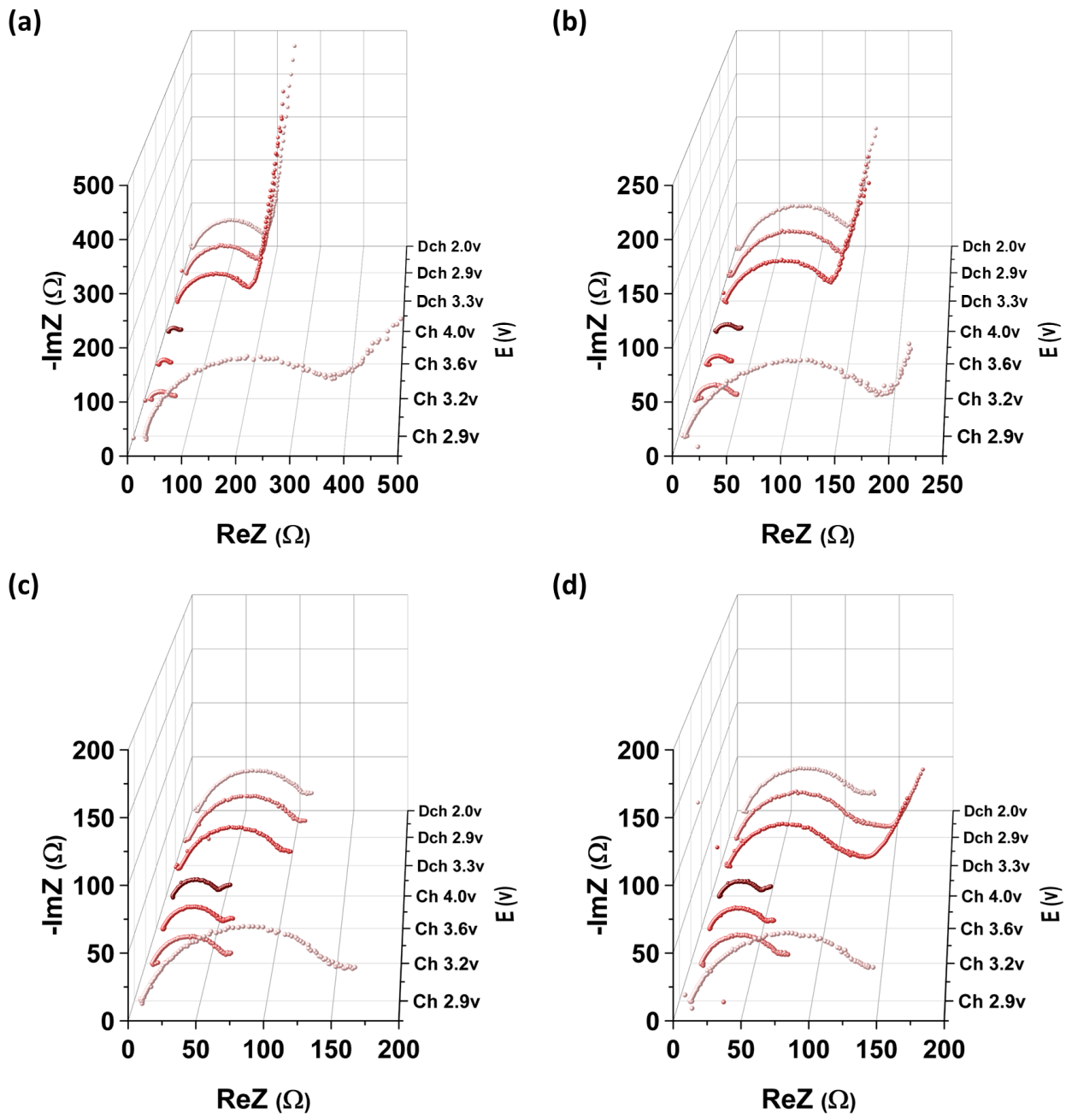

Figure S12. In situ EIS (Nyquist) profiles of 25@FLP-PB recorded at selected SOC during the (a) 1st, (b) 2nd, (c) 5th, and (d) 15th cycles.

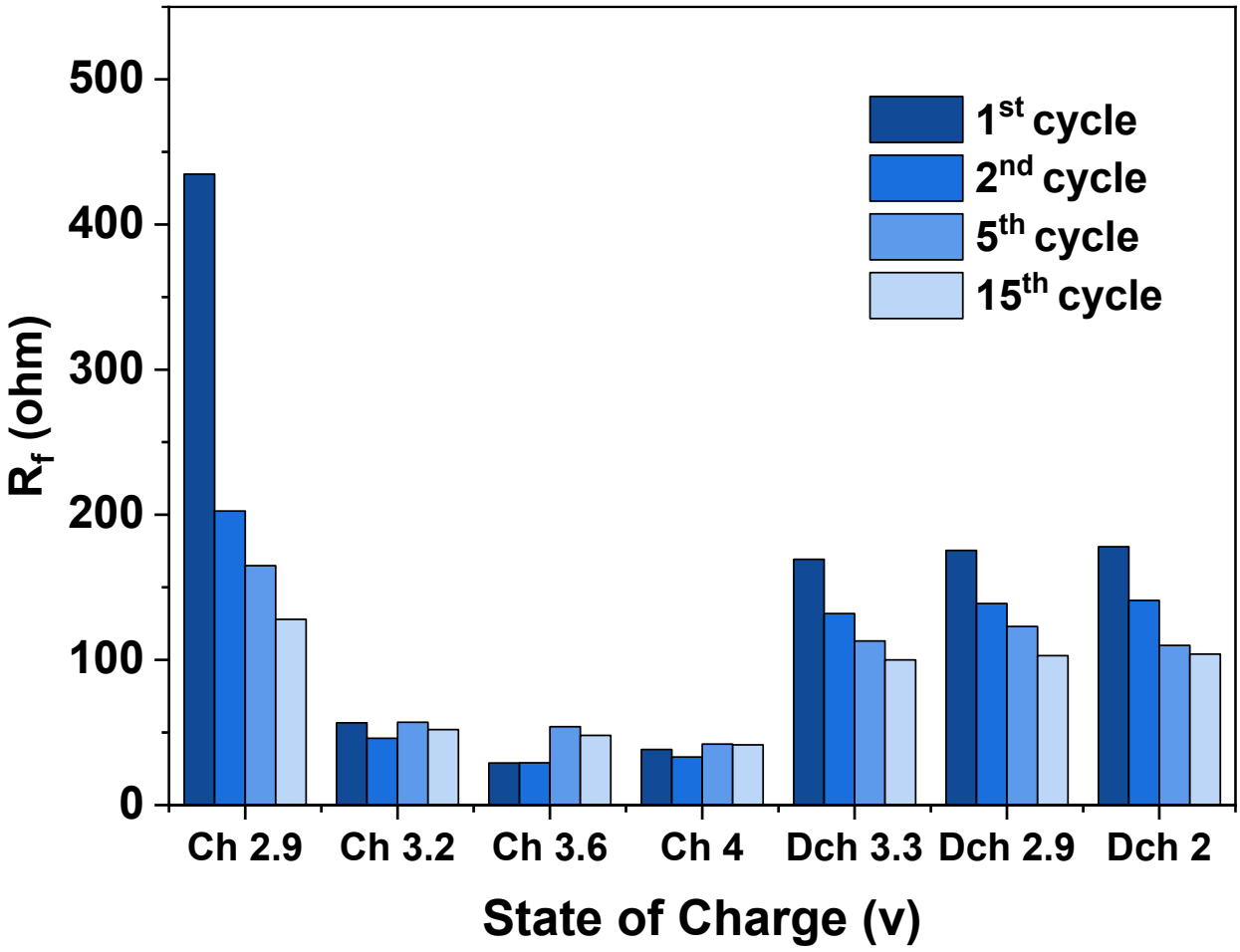

Figure S13. Evolution of the interphase resistance (R_f) at different SOC for pristine PB measured over the 1st, 2nd, 5th, and 15th cycles.

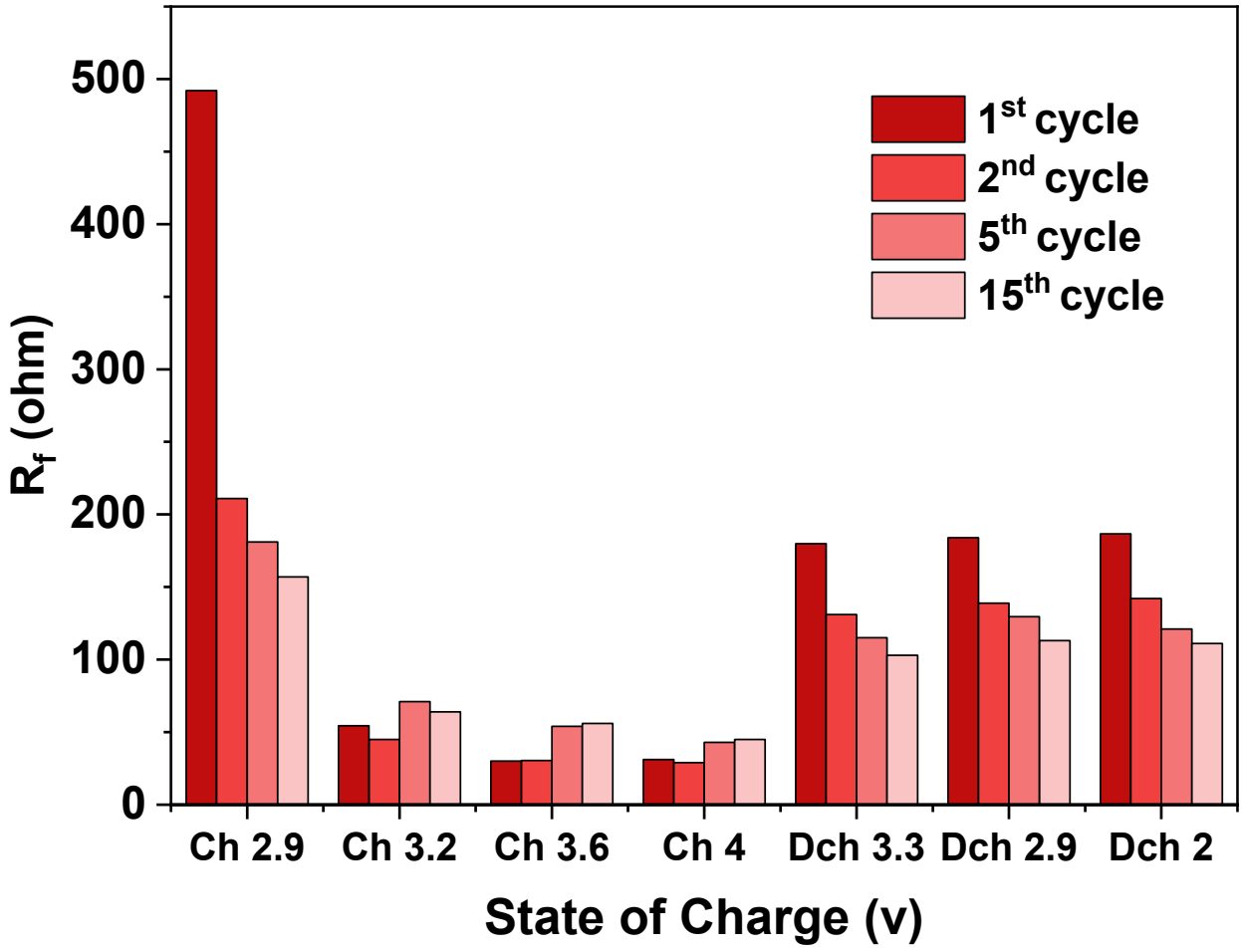

Figure S14. Evolution of the interphase resistance (R_f) at different SOC for coated PB measured over the 1st, 2nd, 5th, and 15th cycles.

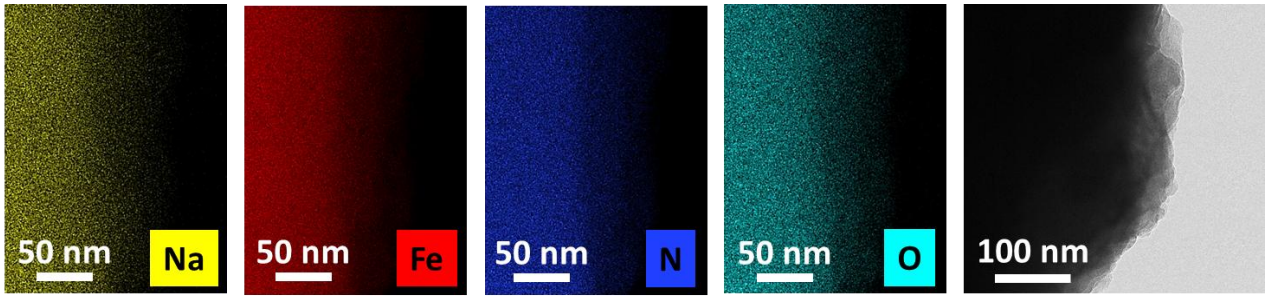

Figure S15. High-resolution TEM images and corresponding EDS elemental mappings of the CEI layer formed on the P-PB cathode after 1000th cycles.

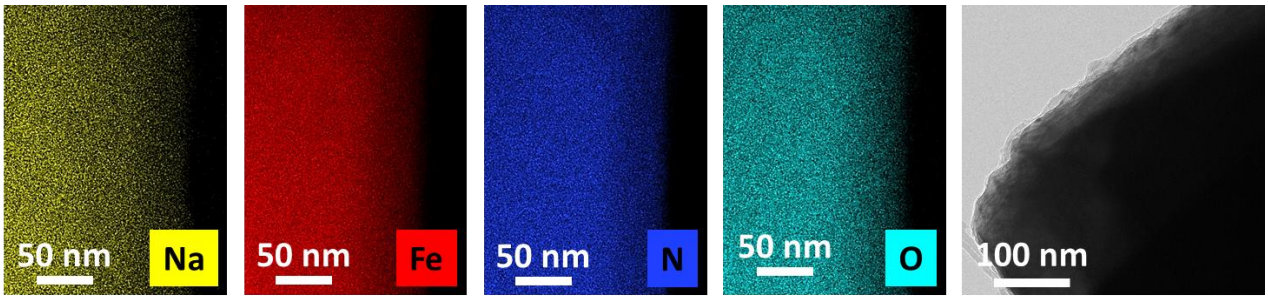

Figure S16. High-resolution TEM images and corresponding EDS elemental mappings of the CEI layer formed on the 25@FLP-PB cathode after 1000th cycles.

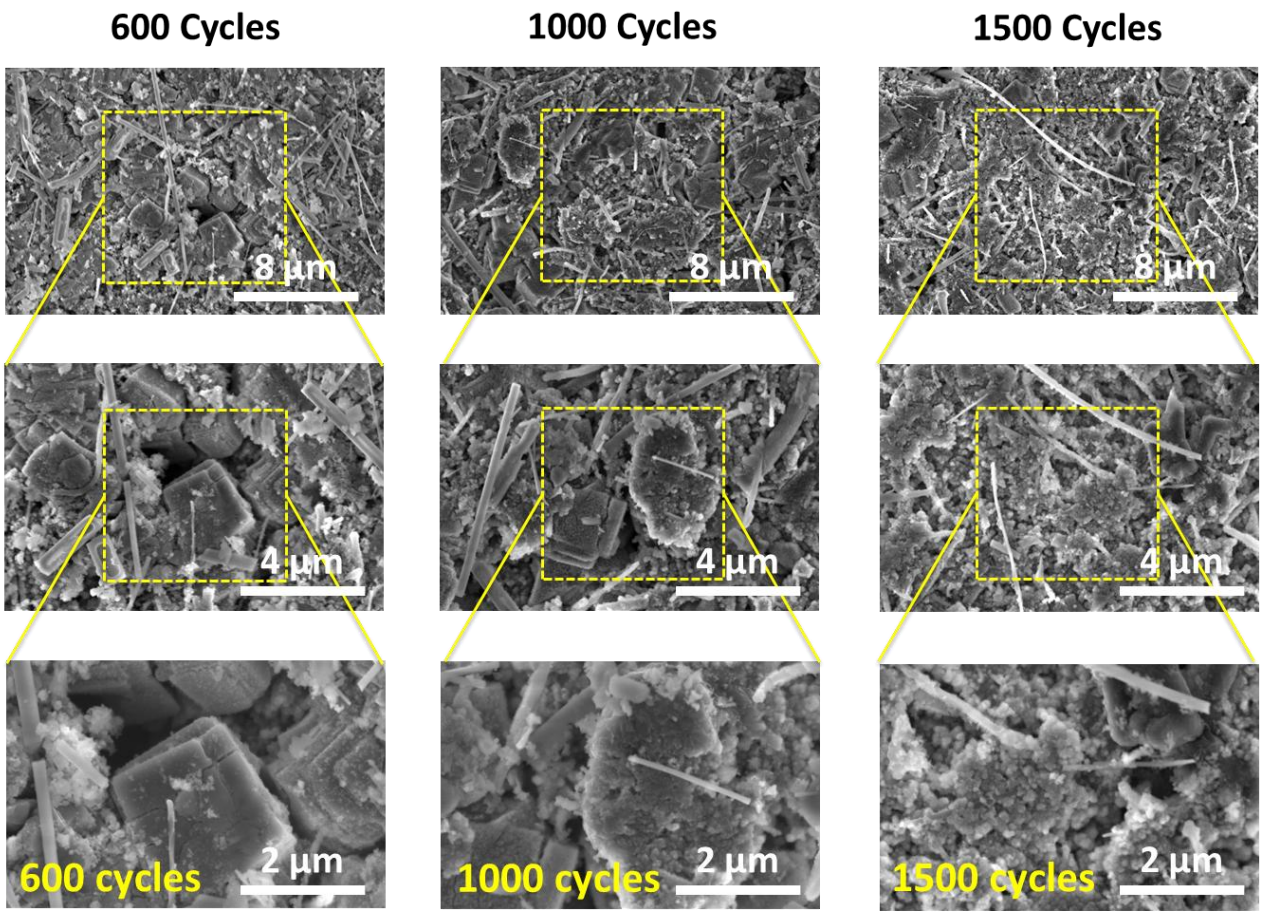

Figure S17. Post-cycling SEM images of the P-PB electrode after 600th, 1000th, and 1500th cycles,

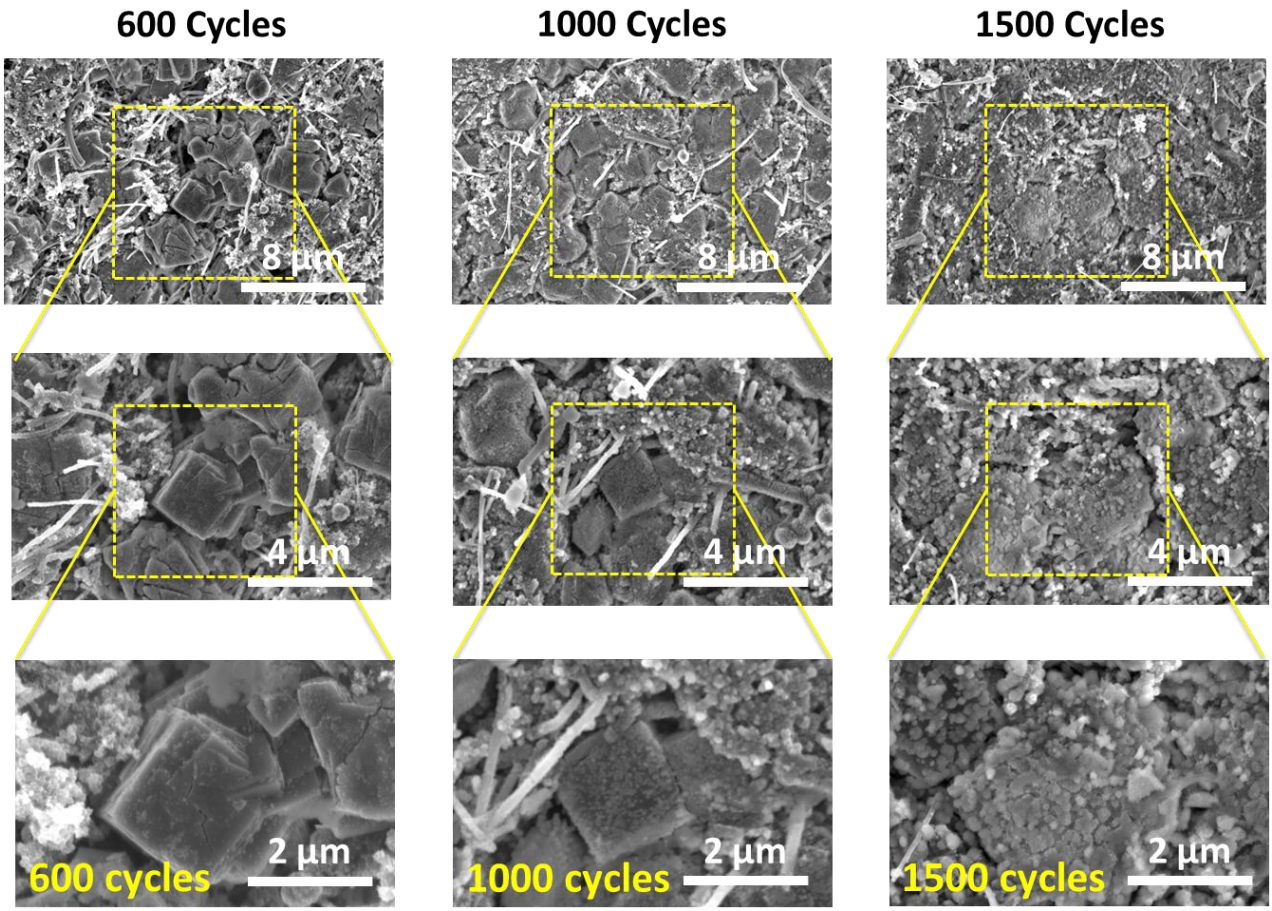

Figure S18. Post-cycling SEM images of the 25@FLP-PB electrode after 600th, 1000th, and 1500th cycles

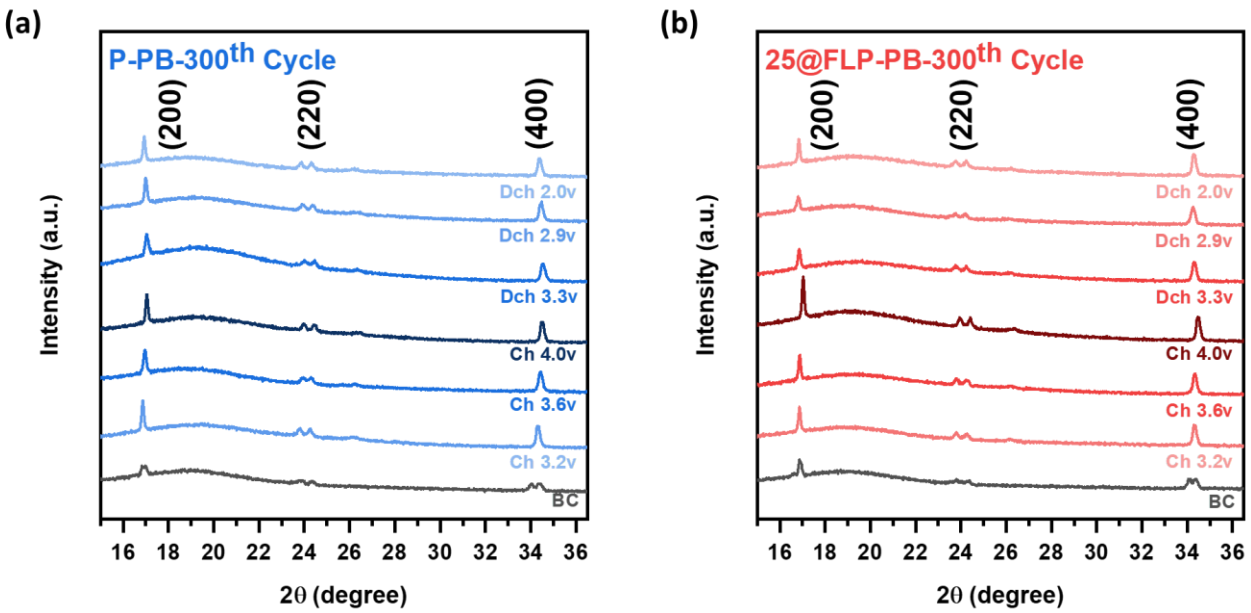

Figure S19. *Ex situ* XRD patterns of P-PB and 25@FLP-PB electrodes at different states of charge and discharge after 300th cycles.

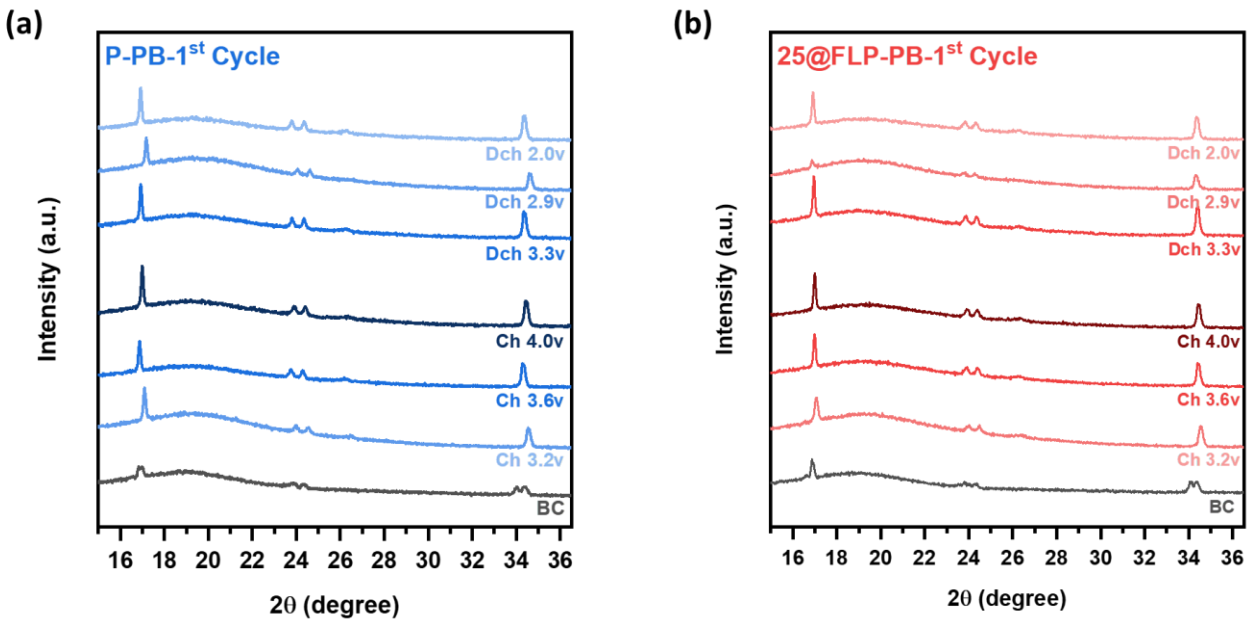

Figure S20. *Ex situ* XRD patterns of P-PB and 25@FLP-PB electrodes at different states of charge and discharge after 1st cycle.

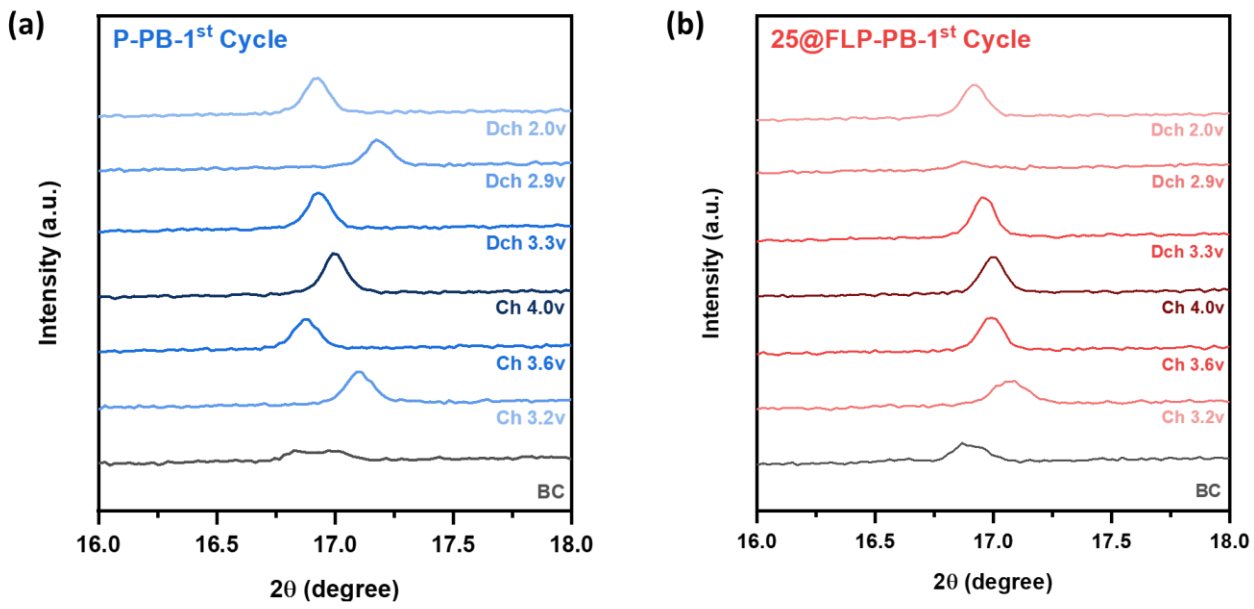

Figure S21. Enlarged view of *ex situ* XRD patterns for the (200) reflection plane for P-PB and 25@FLP-PB samples after 1st cycle.

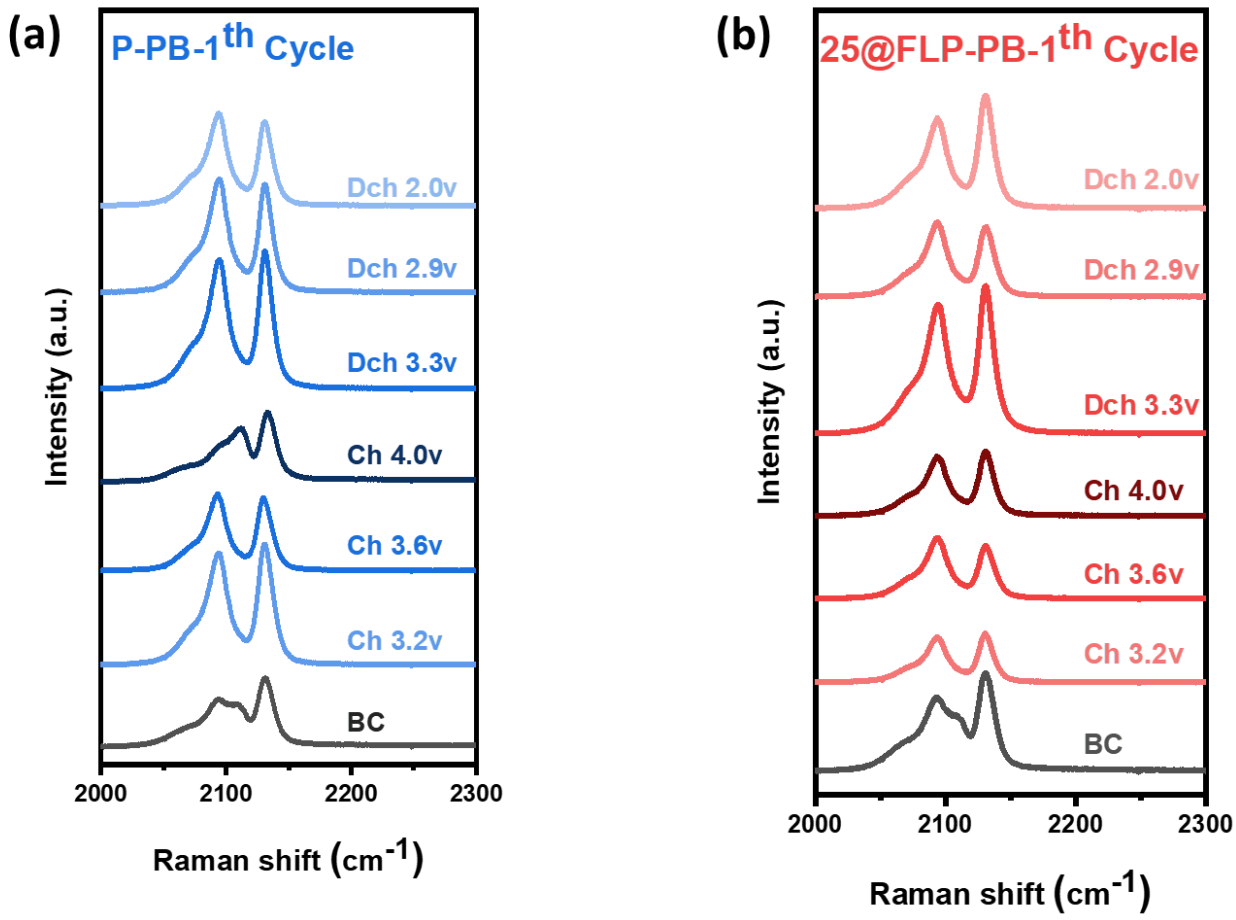

Figure S22. *Ex situ* Raman spectra of the P-PB and 25@FLP-PB electrodes at selected states of charge and discharge during the 1st cycle.

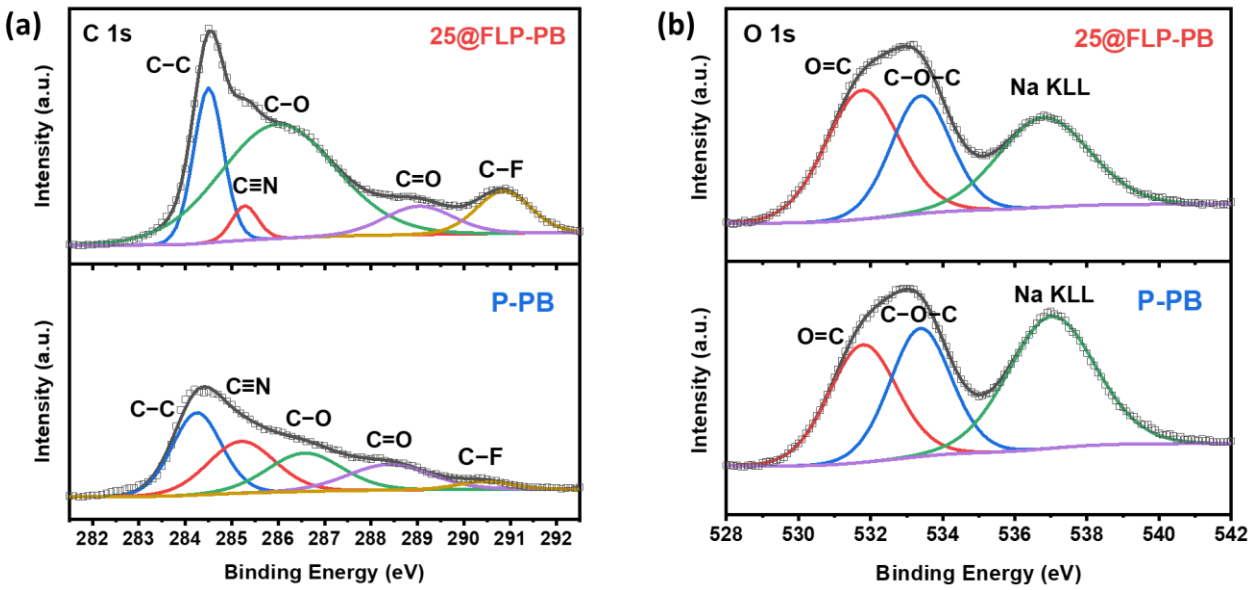

Figure S23. Post-cycling high-resolution XPS spectra for the (a) C 1s and (b) O 1s regions of the CEI on P-PB and 25@FLP-PB electrodes after 1000th cycles.

References

1. Tang, Y., et al., *Polypyrrole-promoted superior cyclability and rate capability of Na x Fe [Fe (CN) 6] cathodes for sodium-ion batteries.* Journal of Materials Chemistry A, 2016. **4**(16): p. 6036-6041.
2. Zhang, Q., et al., *Surface engineering induced core-shell Prussian blue@ polyaniline nanocubes as a high-rate and long-life sodium-ion battery cathode.* Journal of Power Sources, 2018. **395**: p. 305-313.
3. Ye, M., et al., *In-situ construction of a NaF-rich cathode–electrolyte interface on Prussian blue toward a 3000-cycle-life sodium-ion battery.* Materials Today Energy, 2022. **23**: p. 100898.
4. Chen, Z.-Y., et al., *Synergistic modification of Fe-based Prussian blue cathode material based on structural regulation and surface engineering.* ACS applied materials & interfaces, 2022. **14**(38): p. 43308-43318.
5. Xu, C., et al., *Surface Engineering Stabilizes Rhombohedral Sodium Manganese Hexacyanoferrates for High‐Energy Na‐Ion Batteries.* Angewandte Chemie, 2023. **135**(13): p. e202217761.
6. Zhang, Y., et al., *Air-stable prussian white cathode materials for sodium-ion batteries enabled by ZnO surface modification.* ACS applied materials & interfaces, 2024. **16**(13): p. 15649-15656.
7. Fu, X.Y., et al., *Achieving a superior Na storage performance of Fe‐based Prussian blue cathode by coating perylene tetracarboxylic dianhydride amine.* Carbon Energy, 2024. **6**(5): p. e446.